

Supporting Information

Carbon dots-mediated sub-2 nm high-entropy alloys for enhanced hydrogen evolution

Huan Zhuo^a, Qijun Song^a, Chan Wang^{*a}, Han Zhu^{*a}

a. Key Laboratory of Synthetic and Biological Colloids, Ministry of Education, School of Chemical and Material Engineering, Jiangnan University, Wuxi, Jiangsu 214122, P. R. China. E-mail: zhysw@jiangnan.edu.cn; wangchan@jiangnan.edu.cn.

1. Experimental Section

1.1. Materials

Catechol, o-phenylenediamine, urea, citric acid, ascorbic acid (AA), histidine potassium hydroxide (KOH), ruthenium trichloride (RuCl₃), ammonium molybdate, zirconium chloride (ZrCl) and rubidium chloride (RbCl) were purchased from Sinopharm Chemical Reagent Co., Ltd. Potassium hexachloroplatinate (KPtCl₆) was purchased from Suzhou GreatChem Technology Co., Ltd. Oleylamine (OAM) was obtained from Shanghai Meryer Biochemical Technology Co., Ltd.

1.2. Preparation of catalysts

1.2.1. Preparation of CDs

Weigh out 0.3 g of catechol and 0.3 g of ortho phenylenediamine separately. Dissolve them in 10 mL of deionized water, and subject the solutions to sonication until the solids are completely dissolved. Then transfer the solutions into the inner lining of a 25 mL polytetrafluoroethylene (PTFE) high-pressure reaction vessel. Maintain the reaction mixture at 200°C for 6 hours. After the reaction is complete, allow the mixture to cool naturally to room temperature. Subsequently, centrifuge to remove the supernatant liquid, and wash the resulting solid with water. Place the washed solid in a vacuum drying oven overnight to obtain the solid CDs powder.

In addition to catechol and ortho phenylenediamine, CDs-1/2/3/4 were synthesized using different combinations of carbon precursors including catechol and ascorbic acid, catechol and citric acid, catechol and urea, and citric acid and histidine respectively.

1.2.2. Preparation of PtRuMoZrRb HEA NPs

PtRuMoZrRb HEA NPs were prepared by solvothermal process utilizing oleylamine as the solvent. Briefly, 0.035 mmol of the respective metal precursors of Pt, Ru, Mo, Zr, and Rb, were mixed with 10 mg of CDs powder in 5 mL of oleylamine. After sonication until complete dissolution, the mixture was transferred into a 25 mL PTFE high-pressure reactor and maintained at 200°C for 5 hours. After the reaction is complete, and the mixture is naturally cooled to room temperature, a black precipitate is obtained by centrifugation and washed multiple times with a mixture of ethanol and cyclohexane (volume ratio of 1:9). Subsequently, place the washed product in a

constant temperature oven overnight to dry and obtain PtRuMoZrRb HEA NPs black solid powder.

Furthermore, PtRuMoZrRb-1.72/1.79/2.13/3.13 HEA NPs were prepared using CDs-1/2/3/4 under the same experimental conditions.

1.3. Characterization

The microstructure and size vibrations of the catalysts were observed by using transmission electron microscope (TEM, JEM-2100PLUS). Energy dispersive X-ray analysis (EDX) was conducted on a field-emission transmission electron microscope (STEM, Talos F200X G2). The content of various metals within the catalyst was determined by inductively coupled plasma emission spectroscopy (ICP). The structural features of the catalysts were characterized using an X-ray powder diffractometer (XRD, D8), equipped with a Linx array detector. The 2θ scanning range was set from 30° to 80° at a rate of $10^\circ/\text{min}$. The lattice parameter (a) from the (111) peak position was

calculated using Bragg's law and the equation for fcc structures: $2d \times \sin\theta = n \times \lambda$ and $d_{111} = \frac{a}{\sqrt{3}}$, where d is the interplanar spacing, θ is the diffraction has angle (i.e. the θ angle corresponding to the diffraction peak), n is the diffraction order, and λ is the wavelength of the target used ($\lambda = 1.5406 \text{ \AA}$). X-ray photoelectron spectrometer (XPS, Axis Supra) operated at a power of 600 W Al $K\alpha$ radiation. The analysis chamber maintained a high vacuum degree level of 9.8×10^{-10} Torr during the XPS measurements.

1.4. Electrochemical measurements

Electrochemical performance testing was carried out at room temperature (25°C) using a CHI 660D electrochemical workstation with a standard three electrode system. For the electrocatalytic HER, carbon paper loaded with the catalyst serves as the working electrode, while Ag/AgCl electrode and platinum sheet functioned as the reference electrode and counter electrode, respectively. The catalyst ink is prepared by dispersing 2 mg of catalyst sample in a solution comprising 200 μL ethanol and 10 μL 5 wt% Nafion solution. Then, 50 μL of this ink is applied onto carbon paper using a pipette, followed by drying at room temperature to obtain catalyst loaded carbon paper. Quantification of the catalyst loading was performed using an analytical balance with a precision of 0.1 mg. The average catalyst mass loading was determined to be 0.24 mg cm^{-2} . During the electrochemical performance measurements, the potential is converted relative to reversible hydrogen electrode (RHE) using the equation: $E \text{ (vs RHE)} = E \text{ (vs Ag/AgCl)} + 0.197 + 0.0591 \times \text{pH}$. The HER polarization curve was obtained by linear sweep voltammetry (LSV), scanning from 0.01 V vs RHE to -0.5 V vs RHE at a scanning rate of 5 mV/s, with 95% iR compensation to account for the internal resistance of the solution. Electrochemical impedance spectroscopy (EIS) was tested across a frequency range of 0.01 Hz and 10 kHz. All the reference electrode was calibrated for each electrochemical measurement session.

The double layer capacitance (C_{dl}) value was calculated by performing cyclic voltammetry (CV) tests at scan rates of 20 mV/s, 40 mV/s, 60 mV/s, 80 mV/s, and 100 mV/s within the non-Faradaic potential window. The electrochemically active area (ECSA) was computed by dividing C_{dl} by the roughness factor (C_s) ($\text{ECSA} = C_{dl}/C_s$, $C_s = 0.04 \text{ mF cm}^{-2}$). The normalized LSV polarization curve of ECSA was obtained by dividing the geometric area normalized polarization curve by ECSA.

The turnover frequency (TOF) value was calculated by following equation:

$$\text{TOF} = \frac{j \times A}{\alpha \times F \times N_{sur}}$$

where j is the current density at the potential of -100 mV, A is the area of the electrode ($A = 1 \text{ cm}^2$), α is the number of electron transfer ($\alpha = 2$), F is the Faradic constant (96485

C mol⁻¹), n_{sur} is the number of the moles of the exposed active sites. The n_{sur} can be calculated by following equation: $n_{sur} = 2\bar{r} \times \bar{R} \times N_{total}$, \bar{r} is the average radius of the atoms, \bar{R} is the average radius of the catalyst spheres, N_{total} can be calculated by the loading mass of the catalyst.

Catalyst stability was evaluated through accelerated durability testing (ADT) experiments. The specific operation involved depositing the catalyst onto the cut carbon paper, using the Hg/HgO electrode and Pt sheet as the reference electrode and counter electrode respectively, utilizing Nafion 115 membrane as the separator. The tests were performed in a two chamber H-type electrolytic cell filled with 1.0 M KOH electrolyte. Firstly, perform LSV testing before stability experiments, followed by additional LSV measurements after 5000 or 10000 CV cycles within the LSV potential range to evaluate the durability.

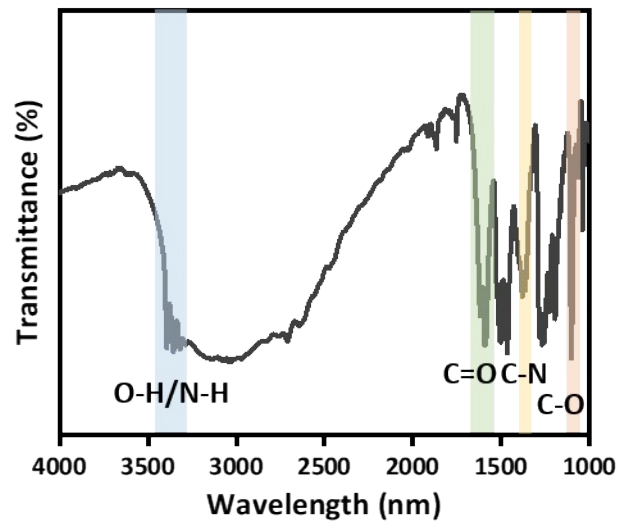


Fig. S1. FTIR spectrum of CDs.

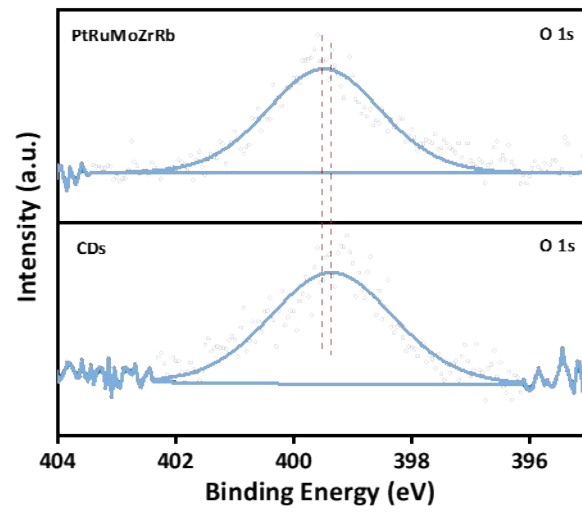


Fig. S2. N 1s XPS spectra of CDs and PtRuMoZrRb HEA NPs.

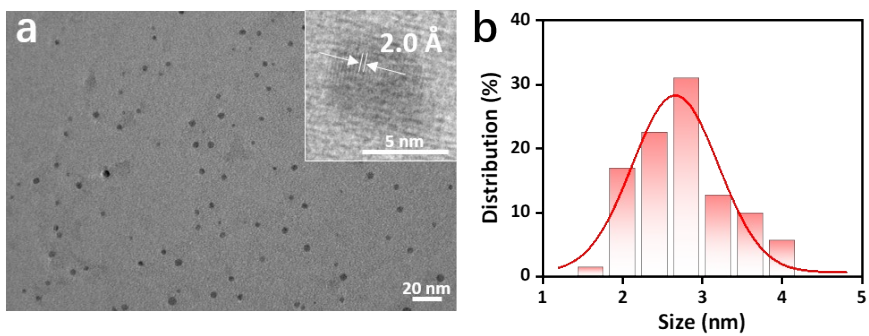


Fig. S3. (a) TEM images of CDs, the inset is the HRTEM image, (b) size distribution histogram of CDs.

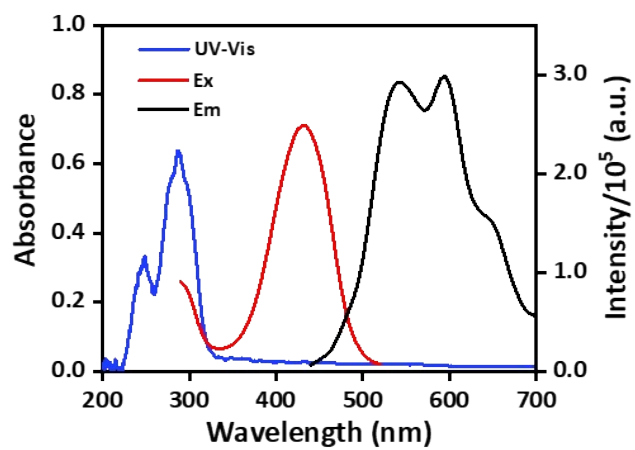


Fig. S4. UV-Vis absorption spectrum (blue line), and fluorescence excitation spectrum (red line) and fluorescence emission (black line) spectra of CDs.

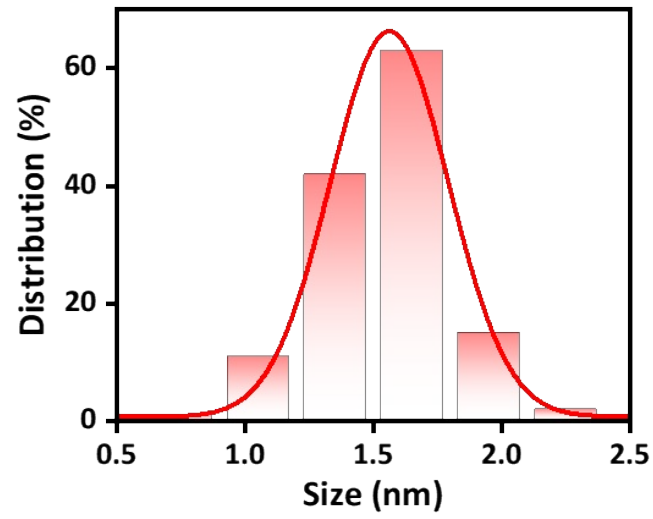


Fig. S5. Size distribution histogram of PtRuMoZrRb HEA NPs.

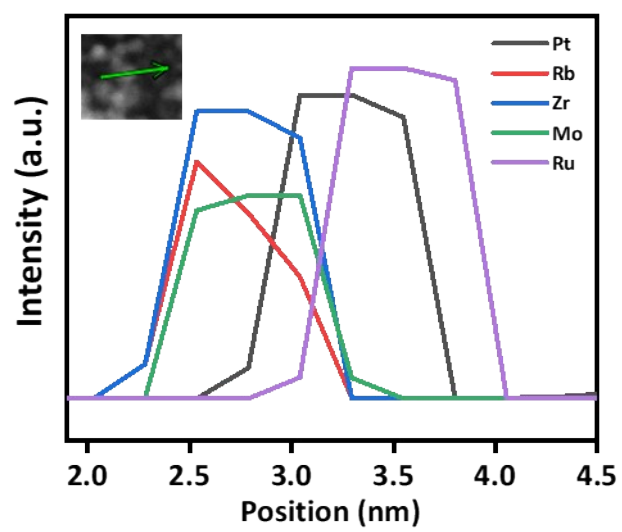


Fig. S6. Line scan STEM-EDS spectra of PtRuMoZrRb HEA NPs.

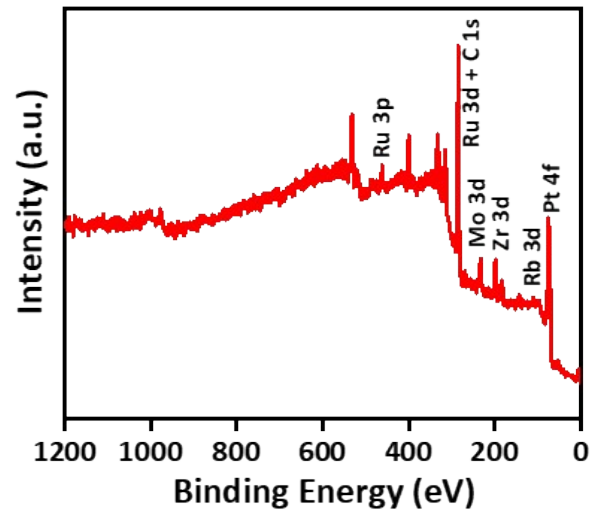


Fig. S7. XPS full spectrum of PtRuMoZrRb HEA NPs

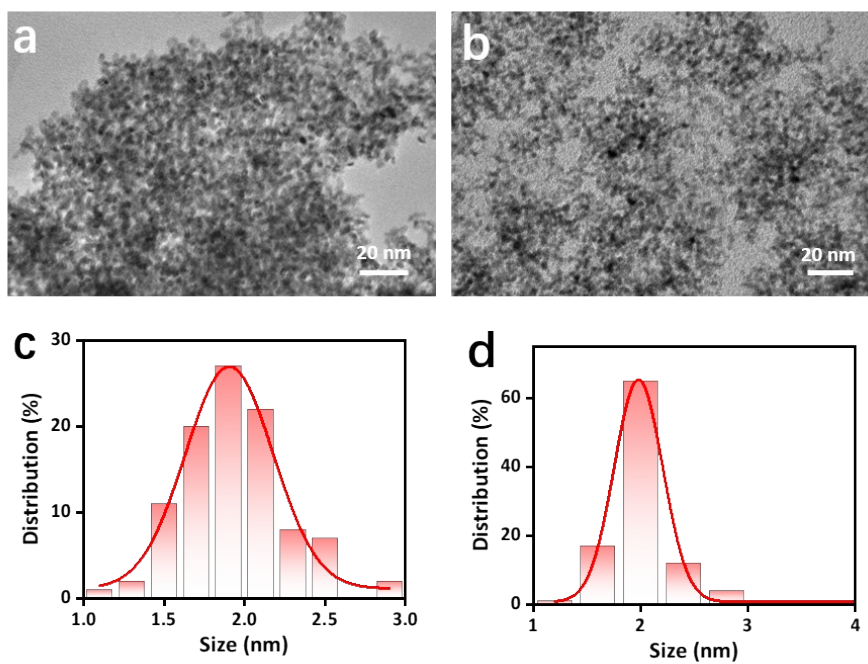


Fig. S8. TEM images of (a) PtRuMo and (b) PtRuMoZr alloys NPs. Size distribution diagram of (c) PtRuMo and (d) PtRuMoZr alloys NPs.

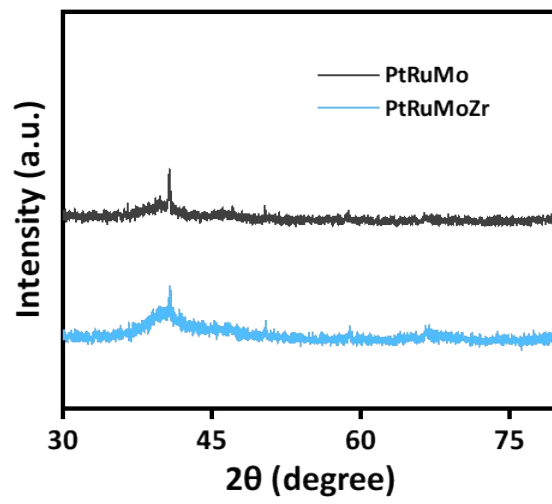


Fig. S9. XRD patterns of (a) PtRuMo and (b) PtRuMoZr alloys NPs.

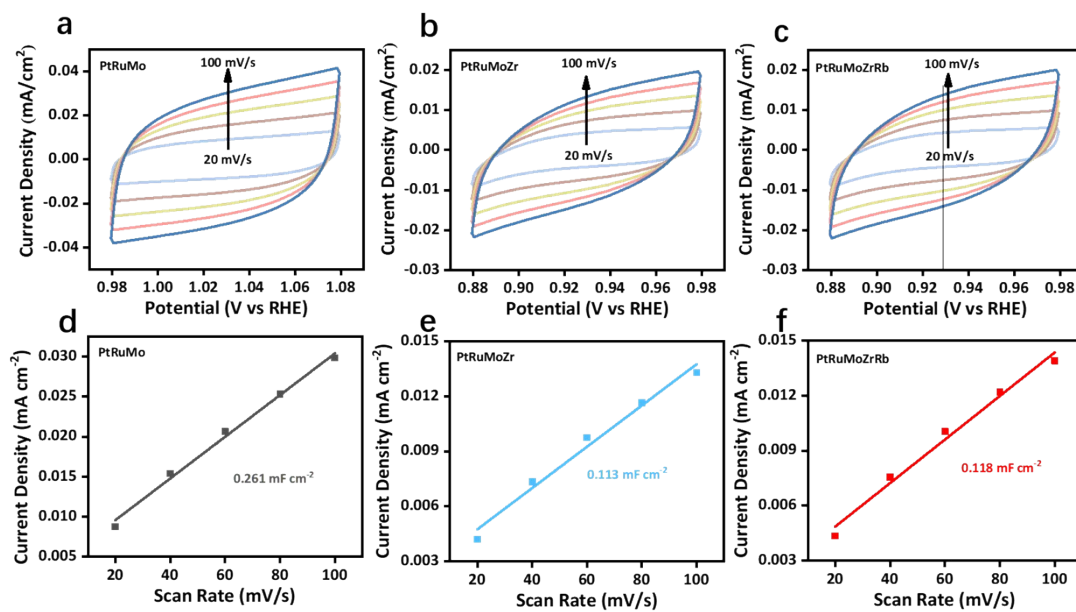


Fig. S10. The cyclic voltammograms profiles obtained on the (a) PtRuMo, (b) PtRuMoZr and (c) PtRuMoZrRb HEA NPs at the sweep rates 20, 40, 60, 80, 100 mV/s respectively. The determination of double layer capacitance of (d) PtRuMo, (e) PtRuMoZr and (f) PtRuMoZrRb HEA NPs.

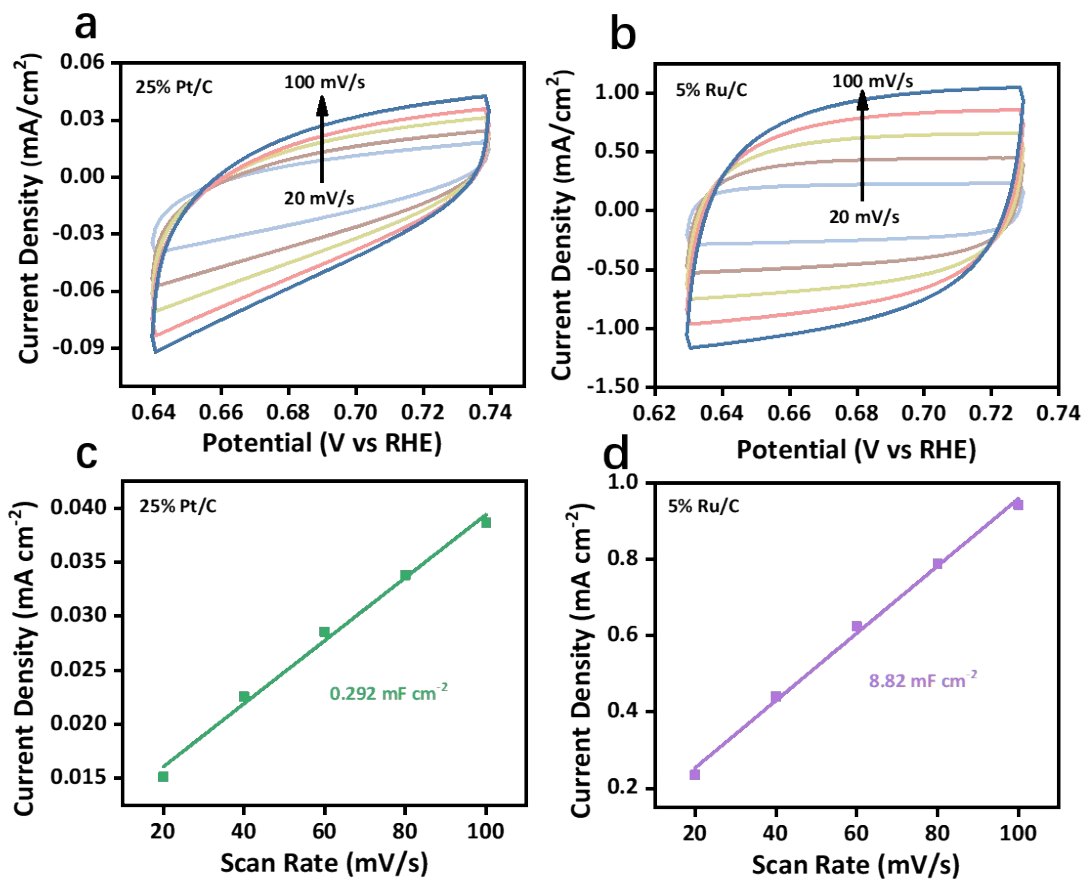


Fig. S11. The cyclic voltammetry profiles obtained on the (a) 20% Pt/C and (b) 5%Ru/C at the sweep rates 20, 40, 60, 80, 100 mV/s respectively. The determination of double layer capacitance of (c) 20% Pt/C and (d) 5%Ru/C.

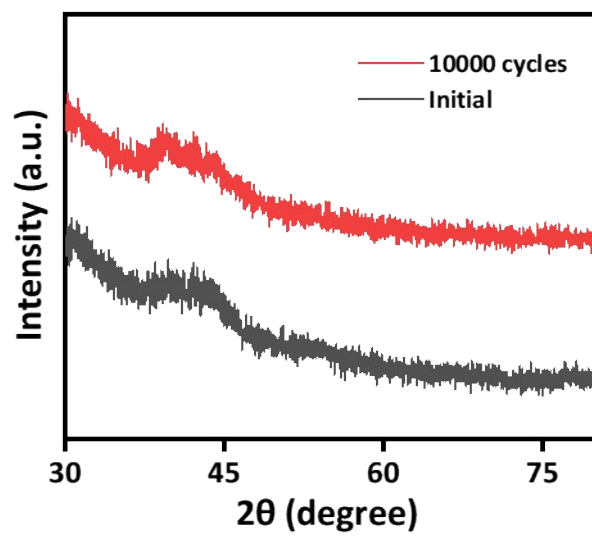


Fig. S12. XRD patterns before and after CV cycles of PtRuMoZrRb HEA NPs.

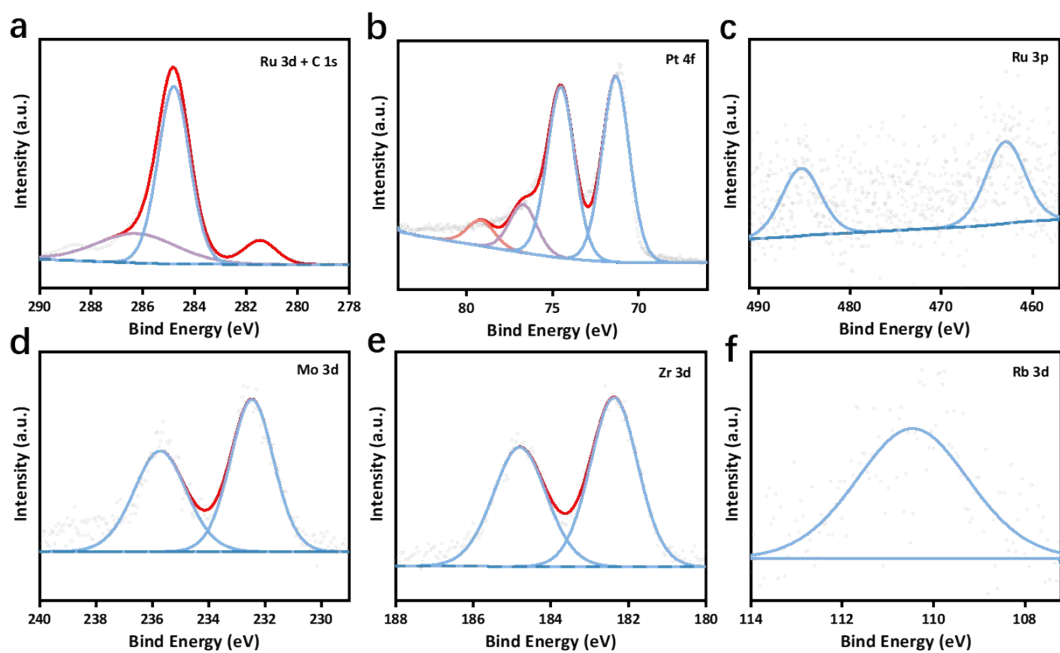


Fig. S13. (a) Ru 3d/C 1s, (b) Pt 4f, (c) Ru 3p, (e) Zr 3d and (f) Rb 3d XPS spectra of PtRuMoZrRb HEA NPs after 10000 CV cycles.

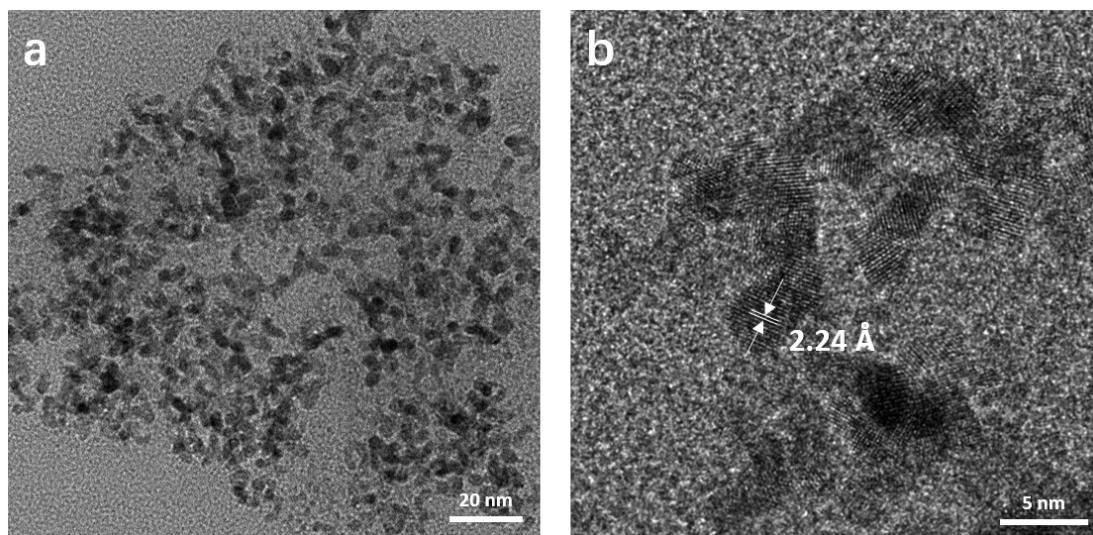


Fig. S14. TEM images of PtRuMoZrRb HEA NPs after 10000 CV cycles.

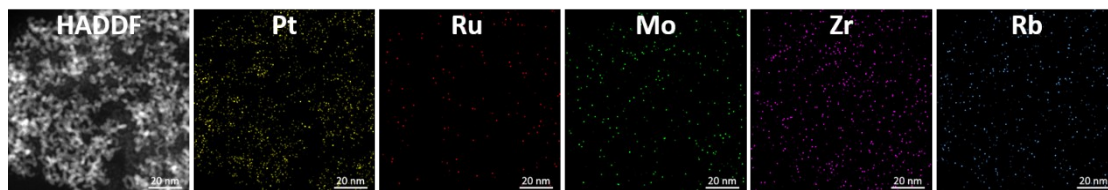


Fig. S15. STEM-EDX mapping of PtRuMoZrRb HEA NPs after 10000 CV cycles.

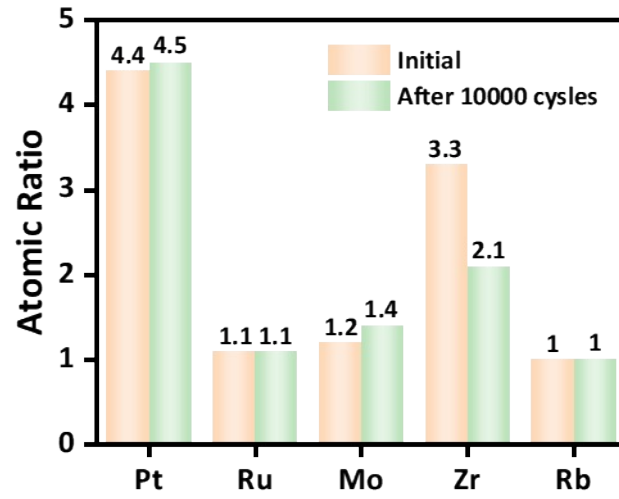


Fig. S16. The atomic ratios of different metals in PtRuMoZrRb HEA NPs obtained from STEM-EDX mapping before and after 10000 CV cycles.

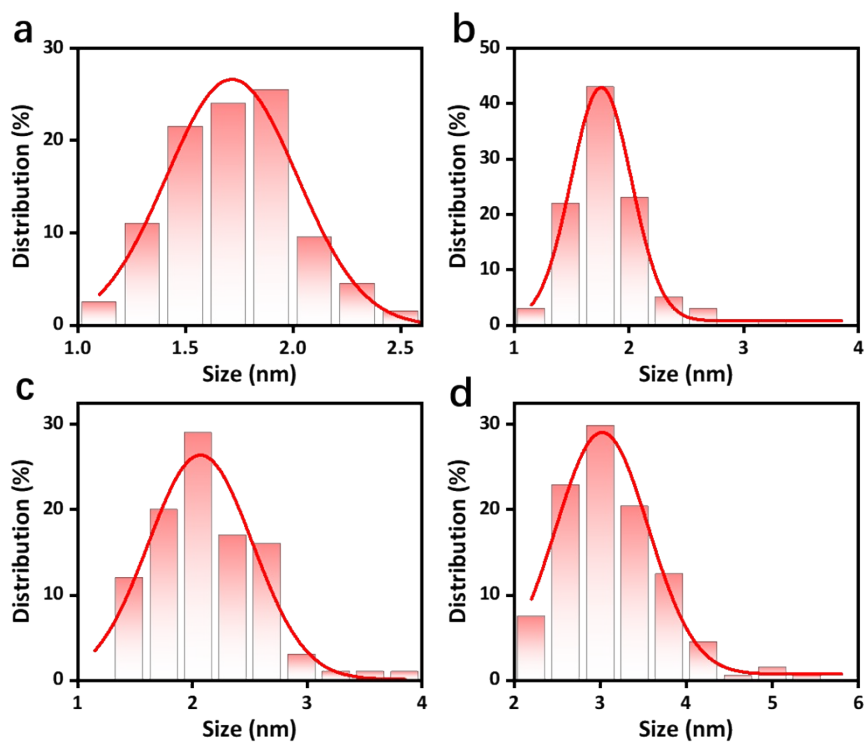


Fig. S17. Size distribution diagram of (a) PtRuMoZrRb-1.72, (b) PtRuMoZrRb-1.79, (c) PtRuMoZrRb-2.13 and (d) PtRuMoZrRb-3.13 HEA NPs.

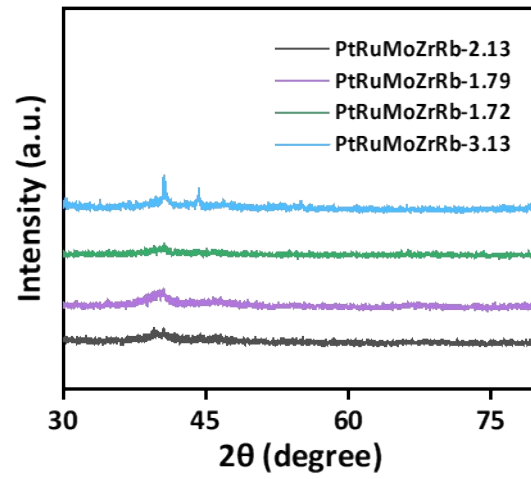


Fig. S18. XRD patterns of PtRuMoZrRb-1.72/1.79/2.13/3.13 HEA NPs.

Table S1. Atomic ratios of PtRuMoZrRb HEA NPs characterized by ICP.

Elements	At%
Pt	7.2
Ru	3.7
Mo	1
Zr	1
Rb	1.3

Table S2. Comparison of PtRuMoZrRb HEA NPs and reported catalysts for HER in 1 M KOH.

Catalysts	TOF (s^{-1})	Potential (mV)	Ref.
PtRuMoZrRb HEA NPs	5.6	100	This work
Pt ₁ -MoL-Mo ₂ C SSAAs	1.24	200	1
Co-P ₃ /S-TiO ₂	1.13	200	2
Ru-Mo solid-solution	0.12	100	3
15 wt% Ir-Ni/NiO@CNT	2.51	100	4
Ru/NC	4.55	100	5
RuNi/CQDs	5.03	100	6
Ru/NG-750	0.35	100	7

Table S3. Comparison of HER performance among some reported catalysts in alkaline media.

Catalysts	η_{10} (mV)	Ref.
PtRuMoZrRb HEA NPs	24	This Work
PtC ₆₀	24.3	8
Ru _{NPs} -RuCr _{APs} -N-C	31	9
CoNi-N/CMF	32.6	10
FeP@CoP	33	11
Pt NPs@CF	35	12
FeCoNiMnRu HEA	37	13
Ni@NCP	42	14
PtNiMnCuMo	44	15
Ru@V-RuO ₂ /CHMS	46	16
Cu-CoS ₂	64	17
Ni-MoB ₂	65.4	18
NiO _x /NF	70	19
V _{0.8} Mo _{0.2} Se _{2-x}	72.3	20
FeCoNiRu-450	100	21

Table S4. A list of the HEAs reported previously.

HEAs	Size (nm)	Ref.
CoMoFeNiCu NPs	~22	22
HEAN/CNT	~20	23
IrRuRhMoW/C	~1.78	24
HEA-1.7	~1.7	25
HEA-QDs	~1.92	26
NiCoMnPt HEAs	~2.6	27
PtRuMoZrRb HEA NPs	~1.54	This Work

Table S5. Comparison of overpotential at 10 mA cm⁻² of various CDs and their synthesized HEA NPs.

Catalysts	η_{10} (mV)	Catalysts	η_{10} (mV)
CDs	597	PtRuMoZrRb-1.54	24
CDs-1	640	PtRuMoZrRb-1.72	39
CDs-2	618	PtRuMoZrRb-1.79	258
CDs-3	501	PtRuMoZrRb-2.13	554
CDs-4	751	PtRuMoZrRb-3.13	/

References

1. L. Xu, Y. Xu, B. Xia, B. Guo, K. M. Kamal, B. Likozar, X. Li, F. Dong, S. Li and Y. Ma, *Adv. Mater.*, 2025, 2502989.
2. S. Qian, T. Jiang, J. Wang, W. Yuan, D. Jia, N. Cheng, H. Xue, Z. Xu, R. Gautier and J. Tian, *ACS Catal.*, 2024, **14**, 18690-18700.
3. Z. Chen, H. Zeng, C. Zhang, H. Cai, Y. Jiang, J. Hu, H. Wang, J. Wang and Y. Cui, *Nano Res.*, 2025, **18**, 94907346.
4. J. Liu, Z. C. Wang, D. Zhang, Y. N. Qin, J. Xiong, J. P. Lai and L. Wang, *Small*, 2022, **18**, 2108072.
5. J. Zhang, P. Liu, G. Wang, P. P. Zhang, X. D. Zhuang, M. W. Chen, I. M. Weidinger and X. L. Feng, *J. Mater. Chem. A*, 2017, **5**, 25314-25318.
6. Y. Liu, X. Li, Q. Zhang, W. Li, Y. Xie, H. Liu, L. Shang, Z. Liu, Z. Chen, L. Gu, Z. Tang, T. Zhang and S. Lu, *Angew. Chem. Int. Ed.*, 2019, **59**, 1718-1726.
7. R. Ye, Y. Liu, Z. Peng, T. Wang, A. S. Jalilov, B. I. Yakobson, S.-H. Wei and J. M. Tour, *ACS Applied Materials & Interfaces*, 2017, **9**, 3785-3791.
8. J. Y. Chen, M. Aliasgar, F. B. Zamudio, T. Y. Zhang, Y. L. Zhao, X. Lian, L. Wen, H. Z. Yang, W. P. Sun, S. M. Kozlov, W. Chen and L. Wang, *Nat. Commun.*, 2023, **14**, 1711.
9. P. Eskandari, S. J. Zhou, J. Yuwono, D. Gunawan, R. F. Webster, Z. P. Ma, H. Y. Xu, R. Amal and X. Y. Lu, *Adv. Mater.*, 2025, 2419360.
10. J. Yu, Y. X. Wang, Y. F. Jing, M. I. Asghar, Y. K. Li, Y. Zhang, Q. Liu, R. M. Li, J. Wang and P. D. Lund, *Chem. Eng. J.*, 2024, **484**, 149406.
11. K. Zhang, J. Jia, E. D. Yang, S. P. Qi, H. Z. Tian, J. X. Chen, J. Li, Y. B. Lou and Y. Z. Guo, *Nano Energy*, 2023, **114**, 108601.
12. Q. Q. Li, Z. Deng, D. F. Tao, J. Y. Pan, W. L. Xu, Z. X. Zhang, H. W. Zhong, Y. H. Gao, Q. Shang, Y. Q. Ni, X. K. Li, Y. T. Chen and Q. Zhang, *Adv. Funct. Mater.*, 2024, **34**, 10.
13. G. B. Liu, C. Song, X. L. Li, Q. S. Jia, P. F. Wu, Z. H. Lou, Y. S. Ma, X. J. Cui, X. Zhou and L. H. Jiang, *Chem. Eng. J.*, 2025, **509**, 151070.
14. J. Kim, H. W. Choi, H. Choi, M. H. Han, S. Bin Kwon, H. S. Oh, H. Y. Kim and D. H. Yoon, *Appl. Catal. B-Environ. Energy*, 2024, **357**, 124324.
15. T. Gu, F. S. Yu, Z. Q. Yu, Y. X. Qi, Y. X. Li, F. Miao and Z. J. Yan, *J. Colloid Interface Sci.*, 2025, **688**, 308-316.
16. Y. P. Li, W. T. Wang, M. Y. Cheng, Y. F. Feng, X. Han, Q. Z. Qian, Y. Zhu and G. Q. Zhang, *Adv. Mater.*, 2023, **35**, 10.
17. Q. Y. Wang, Y. J. Gong, Y. Tan, X. Zi, R. Abazari, H. M. Li, C. Cai, K. Liu, J. W. Fu, S. Y. Chen, T. Luo, S. G. Zhang, W. Z. Li, Y. F. Sheng, J. Liu and M. Liu, *Chin. J. Catal.*, 2023, **54**, 229-237.
18. F. Yang, R. Q. Yao, Z. L. Lang, F. Y. Yu, H. L. Dong, Y. H. Wang, Y. G. Li and H. Q. Tan, *ACS Energy Lett.*, 2023, **8**, 5175-5183.
19. J. H. Jiang, H. J. Dou, M. R. Cao, L. T. Du, Y. Y. Yan, X. D. Wang, C. Z. Chen, L. J. Ye, B. Deng and H. B. He, *Int. J. Hydrog. Energy*, 2024, **51**, 887-894.
20. J. Zhang, J. D. Li, H. J. Huang, W. Chen, Y. Cui, Y. H. Li, W. W. Mao, X. B. Zhu and X. A. Li, *Small*, 2022, **18**, 2204557.
21. K. Huang, J. Xia, Y. Lu, B. Zhang, W. Shi, X. Cao, X. Zhang, L. M. Woods, C. Han, C. Chen, T. Wang, J. Wu and Y. Huang, *Adv. Sci.*, 2023, **10**, 2300094.
22. P. F. Xie, Y. G. Yao, Z. N. Huang, Z. Y. Liu, J. L. Zhang, T. Y. Li, G. F. Wang, R. Shahbazian-Yassar, L. B.

- Hu and C. Wang, *Nat. Commun.*, 2019, **10**, 12.
23. X. X. Zou, J. Y. Xie, Z. Y. Mei, Q. Jing, X. L. Sheng, C. H. Zhang, Y. X. Yang, M. J. Sun, F. T. Ren, L. L. Wang, T. W. He, Y. C. Kong and H. Guo, *Proc. Natl. Acad. Sci. U. S. A.*, 2024, **121**, 9.
 24. H. Luo, L. Li, F. X. Lin, Q. H. Zhang, K. Wang, D. W. Wang, L. Gu, M. C. Luo, F. Lv and S. J. Guo, *Adv. Mater.*, 2024, **36**, 10.
 25. H. Z. Cai, H. P. Yang, S. Z. He, D. Wan, Y. Kong, D. L. Li, X. X. Jiang, X. Zhang, Q. Hu and C. X. He, *Angew. Chem. Int. Ed.*, 2025, **64**, e202423765
 26. H. Zhao, M. Y. Liu, Q. S. Wang, Y. Z. Li, Y. B. Chen, Y. P. Zhu, Z. Y. Yue, J. Li, G. L. Wang, Z. Q. Zou, Q. Q. Cheng and H. Yang, *Energy Environ. Sci.*, 2024, **17**, 6594-6605.
 27. Y. B. Xu, Y. Tian, S. Guo, B. C. Xu, Y. He, Z. J. Zhao, X. Y. Yuan, Y. X. Wang, J. W. Li, X. J. Wang, P. Wang and Z. M. Liu, *Appl. Catal. B-Environ. Energy*, 2025, **365**, 10.